ADVANCED MATERIALS
www.advmat.de

An Intrinsically Micro-/Nanostructured Pollen Substrate with Tunable Optical Properties for Optoelectronic Applications

Youngkyu Hwang, Anupam Sadhu, Sangho Shin, Shin Woei Leow, Ze Zhao, Jingyu Deng, Joshua A. Jackman, Munho Kim, Lydia H. Wong, and Nam-Joon Cho**

There is broad interest in developing photonically active substrates from naturally abundant, minimally processed materials that can help to overcome the environmental challenges of synthetic plastic substrates while also gaining inspiration from biological design principles. To date, most efforts have focused on rationally engineering the micro- and nanoscale structural properties of cellulose-based materials by tuning fibril and fiber dimensions and packing along with chemical modifications, while there is largely untapped potential to design photonically active substrates from other classes of natural materials with distinct morphological features. Herein, the fabrication of a flexible pollen-derived substrate is reported, which exhibits high transparency (>92%) and high haze (>84%) on account of the micro- and nanostructure properties of constituent pollen particles that are readily obtained from nature and require minimal extraction or processing to form the paper-like substrate based on colloidal self-assembly. Experiments and simulations confirm that the optical properties of the pollen substrate are tunable and arise from light–matter interactions with the spiky surface of pollen particles. In a proof-of-concept example, the pollen substrate is incorporated into a functional perovskite solar cell while the tunable optical properties of the intrinsically micro-/nanostructured pollen substrate can be useful for a wide range of optoelectronic applications.

1. Introduction

Polymeric substrates that are affordable, lightweight, and flexible have received considerable attention due to ongoing advances in the flexible and stretchable electronics field.[1–7] There is a growing body of knowledge about how rationally tuning the mechanical strength, optical transmittance, and chemical stability of polymeric substrates can improve the performance of electronic devices such as transistors, sensors, organic light-emitting diodes (OLEDs), solar cells, and energy generators.[8–12] Within this scope, synthetic polymers such as poly(ethylene terephthalate) (PET), polyimide (PI), polyurethane (PU), and poly(dimethylsiloxane) (PDMS) are widely used as flexible substrates for inorganic, organic, and perovskite solar cells due to the ability to finetune material properties along with low cost, high flexibility, and optical transparency.[13–22]

With growing interest in green technologies, naturally abundant materials such as silk and cellulose have been developed as flexible substrates for solar cell applications due to their transparent, eco-friendly, and biodegradable properties.[23–25] Specifically, incorporating nanostructures such as nanofibers and nanopores into natural material substrates can facilitate high levels of light scattering to improve device efficiency. To date, the main focus has been on controlling fibril and fiber dimensions and packing along with chemical modifications in order to modulate light–matter interactions and the degrees of forward and back scattering. For example, cellulose paper consisting of 10 nm diameter nanofibers was fabricated into a transparent substrate with high transmittance (≈90%)

Dr. Y. Hwang, A. Sadhu, Dr. S. W. Leow, Dr. Z. Zhao, J. Deng, Prof. L. H. Wong, Prof. N.-J. Cho
School of Materials Science and Engineering
Nanyang Technological University
50 Nanyang Avenue, Singapore 639798, Singapore
E-mail: LydiaWong@ntu.edu.sg; njcho@ntu.edu.sg
Dr. Y. Hwang, Prof. J. A. Jackman
School of Chemical Engineering
Sungkyunkwan University
Suwon 16419, Republic of Korea
The ORCID identification number(s) for the author(s) of this article can be found under https://doi.org/10.1002/adma.202100566.
Dr. Y. Hwang, Prof. J. A. Jackman
Biomedical Institute for Convergence at SKKU (BICS)
Sungkyunkwan University
Suwon 16419, Republic of Korea
A. Sadhu, Dr. S. W. Leow, Prof. L. H. Wong
Campus for Research Excellence and Technological Enterprise (CREATE)
1 Create Way, Singapore 139602, Singapore
Dr. S. Shin, Prof. M. Kim
School of Electrical and Electronic Engineering
Nanyang Technological University
50 Nanyang Avenue, Singapore 639798, Singapore

DOI: 10.1002/adma.202100566

and high haze (forward light scattering) that was useful for organic solar cell applications.[26] Transparent paper composed of wood fibers with ≈90% transmittance and haze has also been reported.[24]

Notably, recent findings have suggested that "microscale irregularities" within entangled networks of cellulose fibers and fibrils play an important role in contributing to desirable optical properties,[27] hence motivating the exploration of natural materials with distinct morphological features besides fibrous networks to modulate light–matter interactions. Moreover, currently used natural materials such as cellulose require extensive processing, including chemical modification in many cases, to generate fibrils and fibers with desirable properties and to fabricate entangled networks with suitable nanostructured features (Table S1, Supporting Information).[28,29]

Considering these points, pollen grains are a promising natural material option because they are sustainably abundant, hollow microparticles that have species-specific architectural features; for example, sunflower pollen grains have spiky appendages, nanoscale pores, and a tripartite structure.[30,31] Several material science applications of pollen grains have been reported such as drug carriers, 3D scaffolds, pressure sensors, and oil-absorbing sponges.[32–37] Recently, simple methods based on incubating pollen grains in alkaline solutions and that require minimal processing have been developed to transform hard pollen grains into flexible microgel and paper structures.[30,38] There remains an outstanding need to characterize and rationally tune the optical properties of pollen-derived materials and to explore their potential suitability as photonically active substrates with distinct design principles compared to existing natural material substrates that are based on entangled network architectures.

In this study, we report a flexible, paper-like pollen substrate with high transparency (>92%) and high haze (>84%) that is enabled by the intrinsic micro- and nanoscale structural features of constituent pollen grains that facilitate forward light scattering (haze). The pollen-derived substrate is readily fabricated from minimally processed pollen particles using simple and environmentally friendly methods and the substrate was demonstrated to be practically useful for perovskite solar cell applications. Electrodynamic simulations further shed light on how the micro- and nanoscale structural features of pollen grains comprising the paper-like sheet affect haze and provide guidance for how pollen engineering can be useful to create naturally sourced substrates with advantageous properties for a wide range of optoelectronic applications. Importantly, our findings demonstrate a new class of photonically active natural material substrates that move beyond fiber-like network architectures and harness the intrinsically micro-/nanostructural features of self-assembled, colloidal-like biological materials such as pollen-grain microparticles.

2. Results and Discussion

To fabricate a pollen-derived substrate from discrete, granular pollen particles, the fabrication process began with incubating pollen particles in a 10% KOH solution at 80 °C for 2 h under stirring (**Figures 1**a,b and Figure S1, Supporting Information for detailed process; see also the Experimental Section). After washing the pollen particles five times with fresh KOH solution using centrifugation (4500 rpm, 5 min), additional incubation in KOH solution at 80 °C for 3 h reduced the stiffness of pollen particles, which led to particle flattening during the drying process and aided substrate preparation (Figure 1c). After washing the pollen particles five times more with deionized water using a filtration method, the pollen particle solution was poured into a square Petri dish (lateral dimensions of 245 mm × 245 mm), followed by drying at room temperature (RT) for 5 days to generate a paper-like pollen substrate (Figure 1d). The thickness of the pollen substrate was controlled by adjusting the amount of pollen particles within the mold. For example, 5, 10, and 20 g of defatted pollen particles yielded substrates with ≈13, 22, and 32 μm thicknesses, respectively. Moreover, the pollen substrates exhibited high optical transparency and foldability while scanning electron microscopy (SEM) images showed that the top surface still had microscale spikes, which mirrored the morphological features of sunflower pollen particle surfaces (Figure 1e). From a processing perspective, it was verified that the second KOH incubation step is necessary because, in its absence, the constituent pollen particles stayed rigid and the pollen substrate in this alternative case readily delaminated from the Petri dish after fully drying, while also exhibiting a large number of cracks and wrinkles on the surface (Figure S2, Supporting Information).

Based on the fabrication scheme, we prepared non-pressed and pressed pollen substrates (lateral dimensions = 3 cm × 2 cm) that had distinct morphological properties. The mechanically pressed pollen substrate was generated by placing a non-pressed pollen substrate between two flat metal plates, which provided a uniform force distribution across the overall surface, followed by pressing at 80 °C for 40 min in a heat-pressing machine (Figure S3a, Supporting Information). The pressed pollen substrate had a 10% decrease in total thickness compared to that of the non-pressed pollen substrate (Figure S3b, Supporting Information). Moreover, the Young's modulus value of the pollen substrate increased from ≈1.0 ± 0.4 MPa to ≈1.7 ± 0.1 MPa for non-pressed and pressed substrates, respectively, and this greater mechanical strength is consistent with substrate densification due to greater particle–particle cohesion and a decrease in void space between the particles (Figure S4, Supporting Information). While the pressing process decreased the thickness of the pollen substrate and increased mechanical strength, Fourier transform infrared (FTIR) spectroscopic analysis confirmed that there was no change in the chemical properties of the pressed pollen substrate (Figure S5, Supporting Information).

To directly compare non-pressed and pressed pollen substrates, we pressed only half of a pollen substrate and observed striking differences in the optical properties of the non-pressed and pressed sides (**Figure 2**a). When the sample was placed on top of printed paper, the printed contents on the paper were clearly visible through both regions. However, when the pollen substrate was placed 3 cm above the paper, printed contents could only be clearly seen through the pressed region while the contents were hazy and opaque through the non-pressed region (Figure S6, Supporting Information).

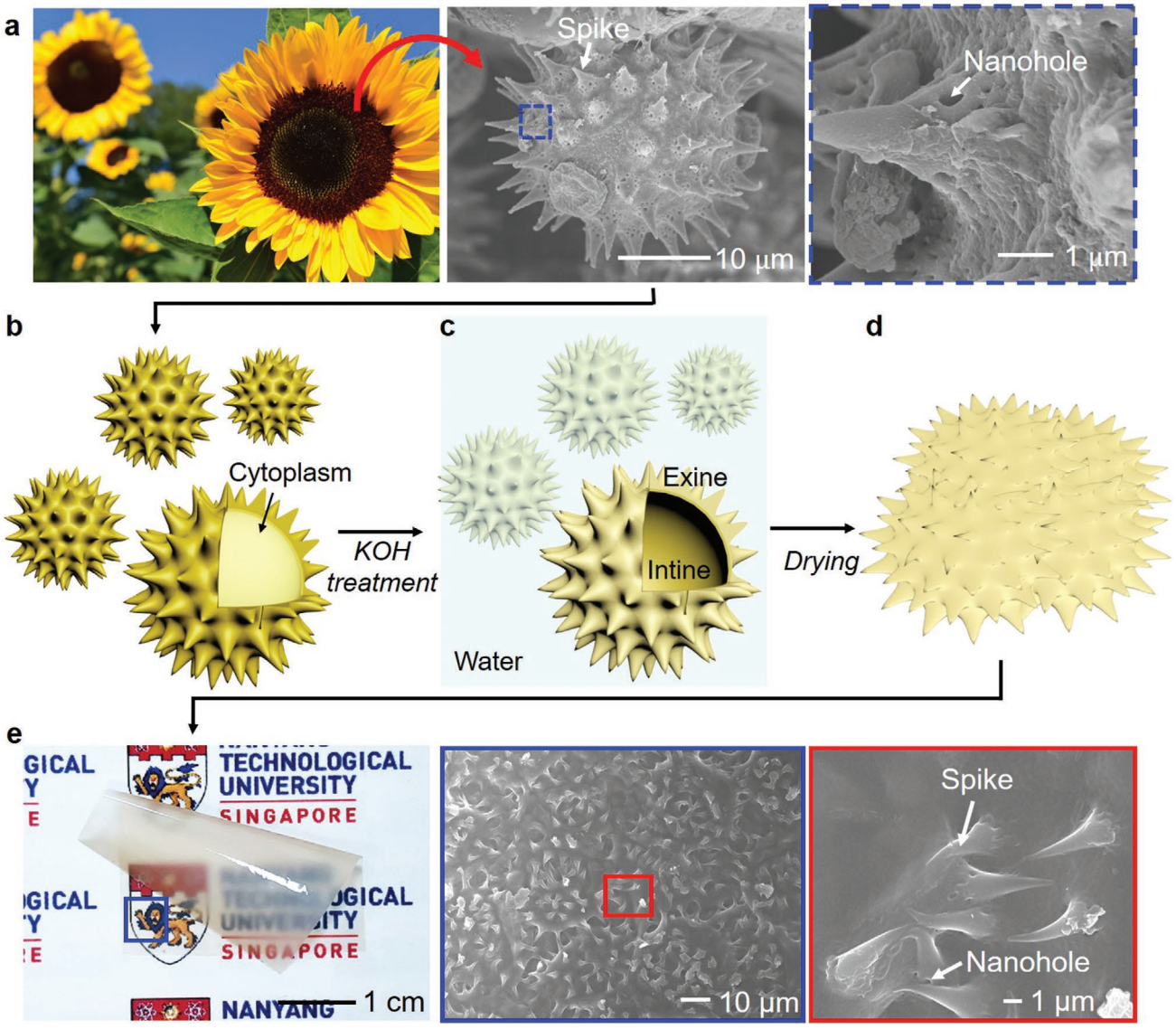

Figure 1. a) SEM images of defatted pollen particles collected from sunflower plants, focusing on microscale spikes and nanoscale apertures. The image of the sunflowers is by Ulleo on Pixabay (CC0). b–d) Schematic illustrations of defatted (b), KOH-treated (c), and dried (d) sunflower pollen particles. e) Photograph of a pollen-derived substrate after drying. The blue and red boxes correspond to magnified SEM images of the selected areas, indicating spike and nanohole features.

We proceeded to measure the total and diffuse transmittance of pollen substrates with various thicknesses by UV–vis spectroscopy measurements (Figures 2b,c). Total transmittance includes directly transmitted and scattered light, which passed through the pollen substrate. While the pressed pollen substrates were thinner, the non-pressed pollen substrates had higher total transmittance than that of the pressed pollen substrate. For example, the non-pressed pollen substrates had 79.0% (32 μm), 89.3% (22 μm), and 92.3% (11 μm) total transmittance at 600 nm wavelength, whereas the pressed pollen substrates had 79.1% (29 μm), 87.4% (19 μm), and 85.8% (9 μm) total transmittance. Regarding direct transmittance, the pressed pollen substrates of 20 and 10 μm thickness showed 82.8% and 83.2% transmittance values at 600 nm wavelength, respectively, which are about ten times higher than the 8% and 9% transmittance values of 23 and 13 μm-thick, non-pressed pollen substrates, respectively (Figure S7, Supporting Information). This result supports that the low reflectivity and high degree of light scattering caused by the surface morphology contribute to high total transmittance.

We also measured the haze, which is an important parameter for optoelectronic devices. The non-pressed pollen substrates had high haze compared to pressed pollen substrates in the visible-light range around 350 to 780 nm (Figure 2d). The haze of the non-pressed pollen substrate was 18-times higher than that of the pressed one. Interestingly, as the thickness of the non-pressed pollen substrate decreased, the haze increased gradually: 64.8%, 83.3%, and 84.0% for 32, 22, and 11 μm-thick substrates, respectively (Figure 2e). As further evidence of light scattering effects, we also observed significant

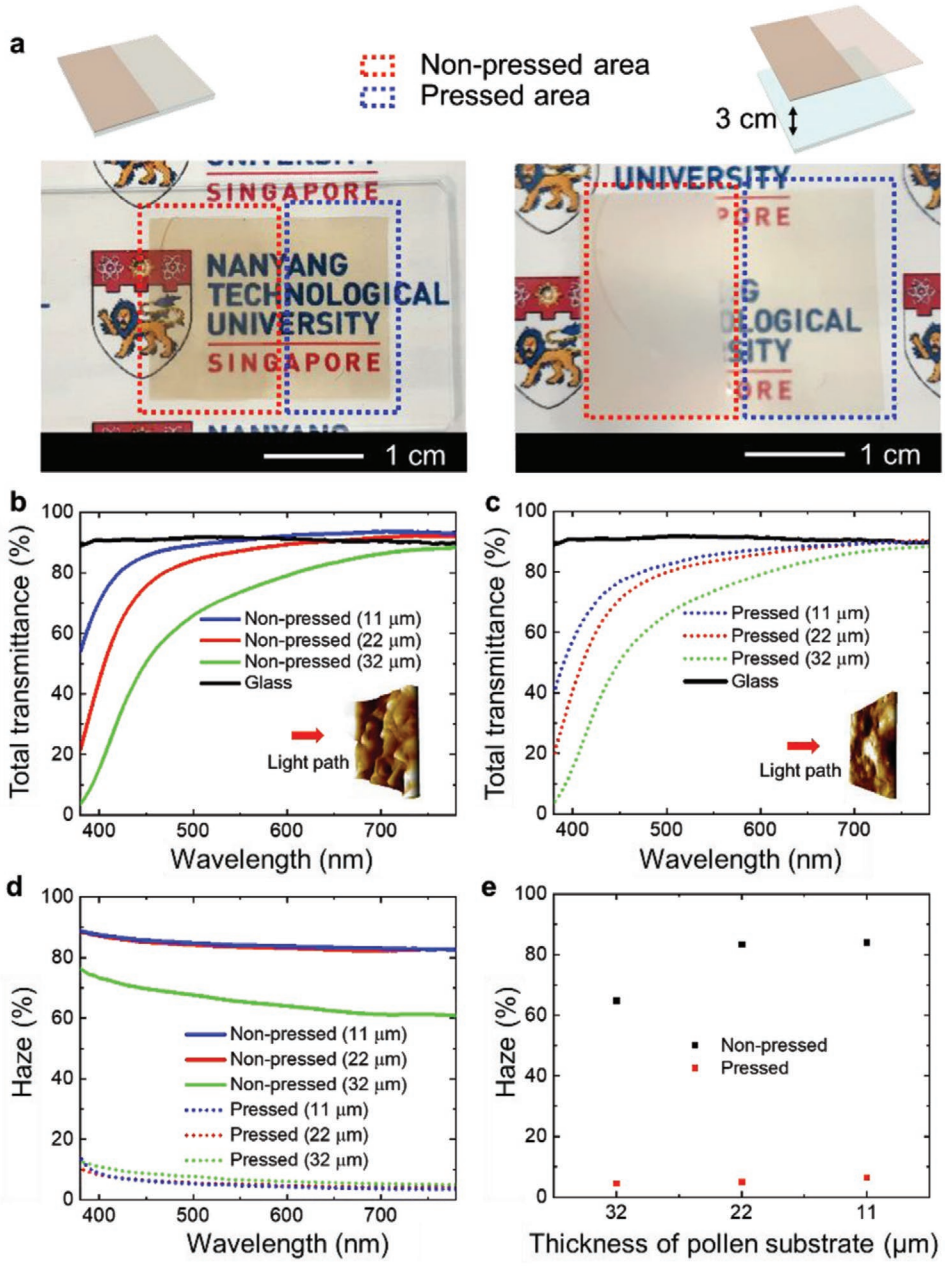

Figure 2. Optical characterization of pollen substrates. a) Left: Photograph of non-pressed and pressed pollen substrates directly on top of printed paper. Right: Photograph of non-pressed and pressed pollen substrate 3 cm on top of printed paper. Note that the thicknesses of the non-pressed and pressed regions were 21 and 19 μm, respectively. b,c) Total transmittance of non-pressed (b) and pressed (c) pollen substrates as a function of substrate thickness. d) Haze of pollen substrates as a function of light wavelength. e) Change in haze property of the pollen substrates before and after pressing.

diffusion of laser light (beam diameter = 0.2 cm, wavelength = 522–542 nm) after passing through the non-pressed pollen substrate (Figure S8, Supporting Information). The observed high haze of the non-pressed pollen substrate could be useful for optoelectronic devices, such as potentially enhancing light absorption within the active layer in a solar cell by extending the light path and collecting light from various angles. Furthermore, the low haze of the pressed pollen substrates, for example, 4.5%, 4.9%, and 6.8% for 29, 19, and 9 μm-thick substrates, respectively, can potentially be useful for display applications such as OLEDs.

To characterize the pollen substrate morphology, we measured the surface roughness of the non-pressed and pressed pollen substrates (thickness = 30 μm, lateral dimensions = 1 cm × 1 cm) by using atomic force microscopy (AFM) (**Figures 3**a,b). The bottom side of the non-pressed pollen substrate had a root-mean-square (RMS) surface roughness of 9.2 nm, while the top side had an RMS surface roughness of 230 nm (Figure 3c). AFM

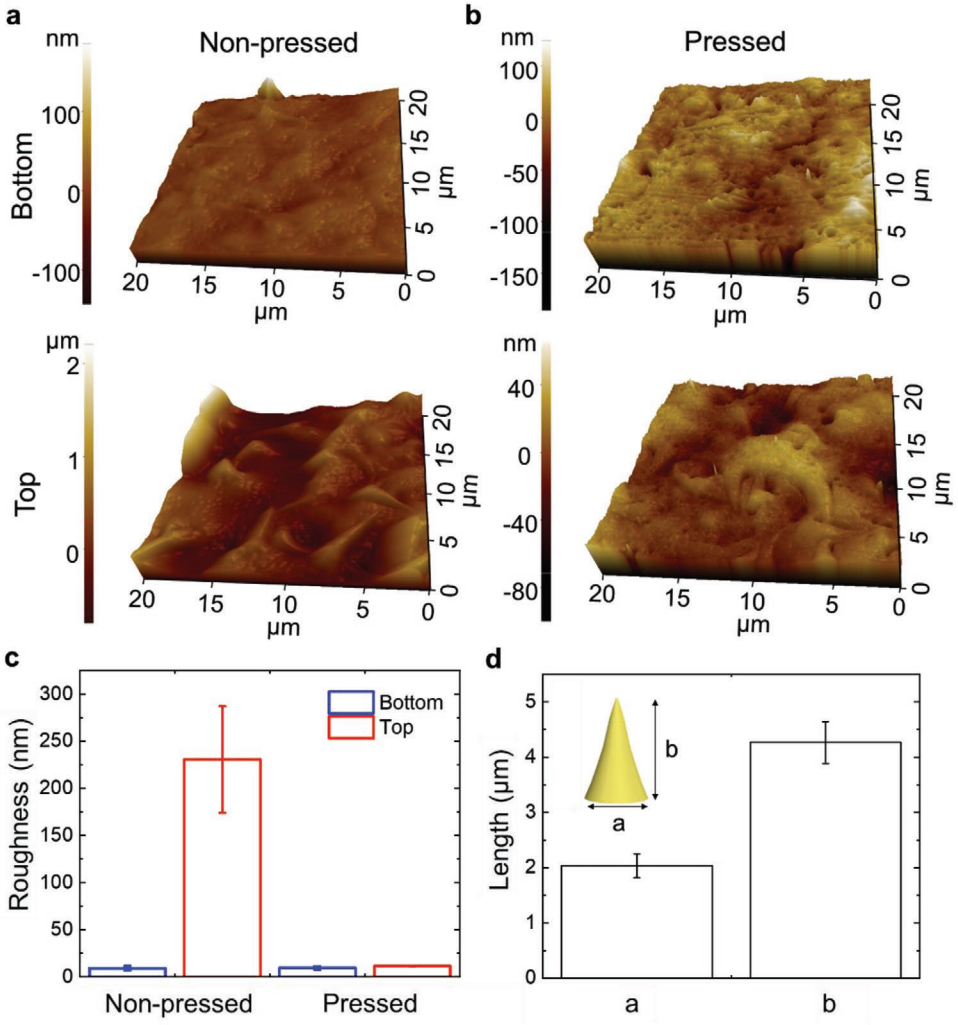

Figure 3. a,b) Surface morphology of the top and the bottom sides of the non-pressed (a) and pressed (b) pollen substrates based on AFM measurements. c) RMS surface roughness of the non-pressed and pressed pollen substrates ($n = 3$). d) Spike dimensions on the outer surface of pollen particles ($n = 6$).

images clearly showed the spike structure with 2.0 ± 0.2 μm diameter and 4.2 ± 0.4 μm height features on top of the non-pressed pollen substrate, while there were no observable structures on the bottom of the non-pressed pollen substrate (Figure 3d). In marked contrast, both sides of the pressed pollen substrate had low RMS surface roughness values (top = 11.3 nm and bottom = 9.4 nm) that were similar to the bottom surface of the non-pressed pollen substrate. In corresponding SEM images, it was verified that the top and bottom surfaces of the pressed pollen substrate exhibited a compressed, smooth morphology, while the top and bottom surfaces of the non-pressed pollen substrate had distinct morphologies and degrees of surface roughness (Figure S9, Supporting Information). These findings support that the low stiffness of the pollen particles induced by KOH treatment led to the successful fabrication of pollen substrates with distinct surface morphologies on the top and bottom sides, while mechanical pressing could further adjust substrate morphology.

To investigate the origin of the light scattering-related haze properties, we performed finite-difference time-domain (FDTD) simulations and examined how the distinct surface morphologies of pressed and non-pressed pollen substrates affect light–matter interactions. The bulk material properties of the pollen substrates were characterized using ellipsometric measurements, from which wavelength-dependent refractive index (n) and extinction coefficient (k) values were obtained, while the nanoscale surface roughness features of the top surface of the pollen substrates were modeled based on the AFM data (Figures S10 and S11, Supporting Information).

Figure 4 shows the schematic of the simulation conditions and distribution of the light intensity in the non-pressed and pressed pollen substrates at various incident light angles. In the case of a 90° incident light angle, the non-pressed pollen substrate showed a similar light-intensity pattern compared to that of the pressed pollen substrate, but the light intensity in the B line (1 μm above the bottom surface, black dotted lines) was higher than that of the pressed one (Figures 4a,b). Interestingly, upon reducing the light angle from 60° to 30°, the decrease in light intensity of the non-pressed pollen substrate was appreciably smaller than that of the pressed pollen substrate

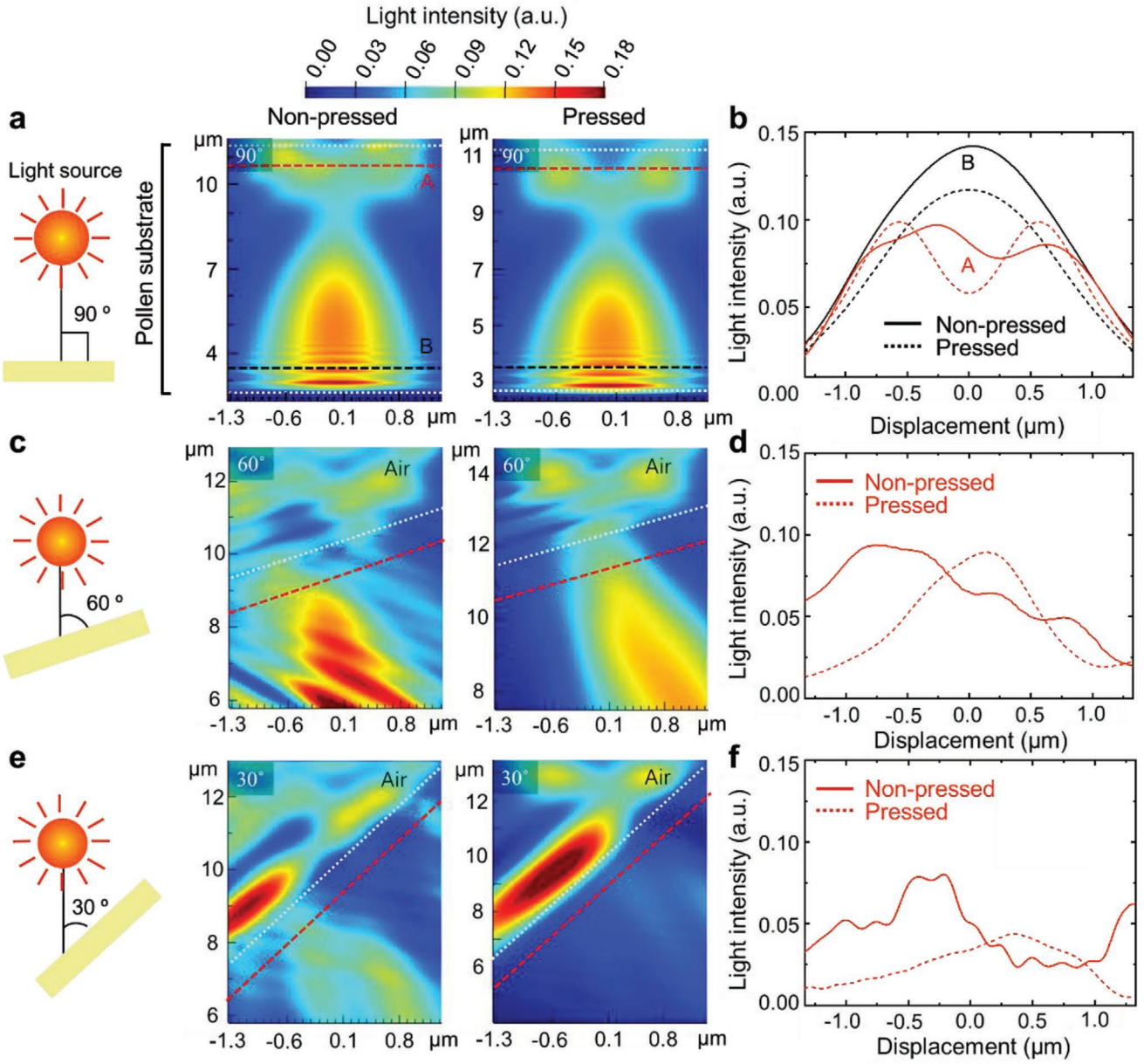

Figure 4. FDTD simulations for modeling haze properties of pollen substrates in air. a) Setup of the FDTD simulation conditions and light intensity distribution maps for non-pressed (thickness = 11 μm) and pressed (thickness = 9 μm) pollen substrates at an incident light angle of 90°. The two dashed white lines in the maps correspond to the top and bottom surfaces of the pollen substrates. The red and black lines labeled with A and B indicate 1 μm distances beneath the top surface and above the bottom surface, respectively. b) Cross-sectional profiles of light intensity at an incident light angle of 90°. c–f) Corresponding simulation results are presented for incident light angles of 60° (c,d) and 30° (e,f), respectively. The dashed white and red lines represent the top surface and a 1 μm distance beneath the top surface, respectively.

(Figures 4c–f). For example, in the 30° incident angle case, strong light intensity was observed at the interface between air and the pressed pollen substrate, while there was negligible light intensity inside the substrate. By contrast, relatively strong light intensity occurred inside the non-pressed pollen substrate. This result indicates that haze-related light scattering arises from micro/nano structures within the pollen substrates that can increase light penetration by reducing light reflection, and hence emphasizes the importance of the pollen architecture in contributing to the optical properties of the substrate.

To demonstrate practical utility in a proof-of-concept example, we evaluated the performance of a perovskite solar cell on the pollen substrate (**Figure 5**a). The process began with the deposition of ZnO (100 nm) as a buffer layer on the pollen substrate (11 μm), which was attached to a glass substrate (see the Experimental Section for the detailed process and Figure S12, Supporting Information). Indium tin oxide (ITO) (500 nm) was sputter-deposited as a transparent electrode, followed by ZnO deposition (100 nm), which is an electron transport layer (ETL) and hole blocking layer. Next, perovskite

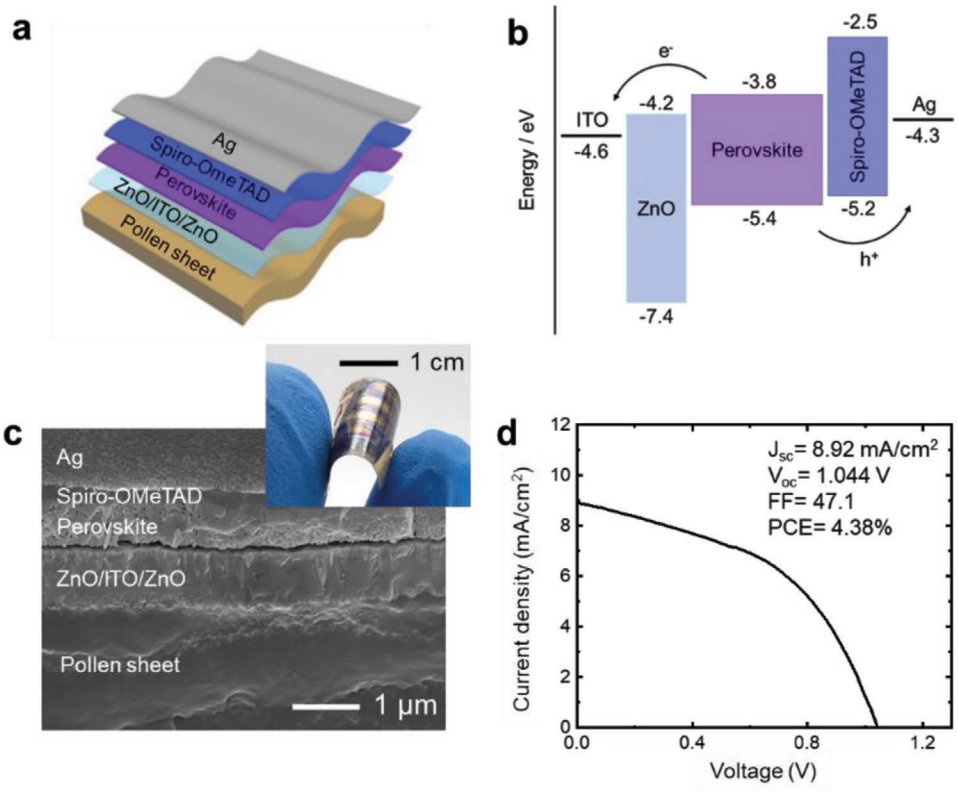

Figure 5. a) Schematic illustration of the perovskite solar cell on the non-pressed pollen substrate. b) Energy band diagram of the device. c) Cross-sectional SEM image of layer stacking in the device. Inset shows a photograph of the flexible device. d) Current density–voltage (*J*–*V*) curve of a representative perovskite solar cell on the non-pressed solar cell under AM 1.5G illumination.

(600 nm) and Spiro-OMeTAD (300 m) layers were coated on the ZnO layer by spin coating, which functions as an active layer and as a hole transport layer (HTL), respectively. Finally, deposition of an Ag electrode (100 nm) with rectangular shape via a stencil mask was performed and formed an electrical contact on the top surface. Figures 5b,c show the energy band alignment between the layers in the device and the final structure of the flexible perovskite solar cell. The performance of this device indicates a power conversion efficiency (PCE) of 4.38% with an open-circuit voltage (V_{oc}) of 1.044 V, short-circuit current (J_{sc}) of 8.92 Ma cm^{-2}, and fill factor of 47.1%. The PCE is among the highest values reported for a perovskite solar cell on a biologically derived material substrate.[39–43] These results indicate that the pollen substrate is compatible with perovskite solar cell function, while the operating performance could be further improved in future work by reducing the thickness of the perovskite and Spiro-OMeTAD layers and/or by optimizing the electrode/ETL layers to enhance charge extraction and series resistance among various design possibilities.

3. Conclusion

We have developed a pollen-derived flexible substrate with high transparency and high haze for optoelectronic applications and demonstrate its utility within a perovskite solar cell as an application example. Importantly, the intrinsic micro- and nanoscale structural features of pollen particles were shown to be critical for modulating light–matter interactions, including reduced light reflectance and increased forward light scattering. In addition, the flat bottom surface of the pollen substrate was useful for material fabrication within complex devices. While other types of natural materials have been used as photonically active substrates in past studies, a unique feature of pollen-based materials is that they possess micro- and nanoscale structural properties stemming from constituent pollen particles, which form the paper-like substrates through colloidal self-assembly as opposed to the conventional case of entangled networks of fibers and/or fibrils, and these structural features of the pollen substrate enable versatile and tunable optical properties without the need for extensive processing. Hence, intrinsically micro-/nanostructured pollen substrates are excellent candidates to replace synthetic plastic substrates and could lead to a new class of environmentally friendly optoelectronic device components.

4. Experimental Section

Preparation of Pollen Substrate: 20 g of defatted sunflower pollen (Helianthus annuus L, Greer Laboratories Inc., Lenoir, NC, USA) was mixed with 10 w/v% KOH (40 mL) under stirring at 80 °C for 2 h in a fume hood. The suspension was then centrifuged at 4500 rpm for 5 min to remove the supernatant. The sample was washed five times with fresh 10 w/v% KOH, followed by centrifugation at 4500 rpm for 5 min.

To decrease the stiffness of the pollen particles, the sample was topped up to a total volume of 40 mL with fresh KOH solution, followed by incubation at 80 °C for 3 h in an oven. After removing the supernatant by centrifugation at 4500 rpm for 5 min, the pollen particles were collected using a filter mesh with 10 μm pore size and then rinsed with deionized water until the solution pH reached a value of 7. The resulting pollen particles constituted a microgel, which was poured into a square Petri dish with lateral dimensions of 245 mm × 245 mm, followed by drying under ambient conditions for 5 days. The pressed pollen substrate was prepared by placing the pollen microgel substrate between four PET films (thickness = 100 μm) and two stainless steel plates (thickness = 1 mm, lateral dimensions = 300 mm × 300 mm) at 80 °C for 40 min using a heat pressing machine. The as-prepared samples were stored in a dry box at a humidity level around 15%.

Material Characterization of Pollen Substrate: Optical transmittance was measured by a UV–vis spectrometer (UV-2700, Shimadzu, Kyoto, Japan) and a UV–vis-NIR spectrophotometer with integrating sphere (Lambda 950, PerkinElmer, Waltham, MA, USA). SEM images were obtained by a JSM-7600F Schottky field-emission scanning electron microscope (JEOL, Tokyo, Japan) at an accelerating voltage of 5.00 kV. Chemical analysis was performed by FTIR spectroscopic analysis (Frontier, PerkinElmer) with a diamond cell attenuated total reflection accessory module. AFM images and surface roughness measurements were obtained using an NX-10 instrument (non-contact mode, scan area = 20 μm × 20 μm, scan rate = 0.2–0.5 Hz, Park Systems, Suwon, Republic of Korea) with an aluminum-reflex-coated silicon cantilever (PPP-NCHR, spring constant of ≈42 N m^{-1}, Nanosensors, Neuchatel, Switzerland). The wavelength-dependent refractive index (n) and extinction coefficient (k) values of pollen substrates were determined by ellipsometry measurements (M-2000 ellipsometer, J.A. Woollam, Lincoln, NE, USA). Tensile mechanical testing was performed using a Dynamic Mechanical Analyzer (DMA Q800, TA Instruments, New Castle, Delaware, USA) and the experiments were conducted at RT with rectangular-shaped samples (20 mm × 5 mm × 0.025 mm) under a tensile rate of 1 N min^{-1} until failure. All data were processed with the Universal Analysis 2000 software package (TA Instruments, New Castle, Delaware, USA).

FDTD Simulations: The distribution of light intensity in both non-pressed (thickness: 11 μm) and pressed (thickness: 9 μm) pollen substrates was simulated by the FDTD method to characterize the effects of pollen substrates on light scattering at various incident angles ranging from 30° to 90°. Light–matter interactions due to pollen spikes, composed of micro/nano structures with a surface roughness of greater than 50 nm, or correlation length of less than 100 nm, and extra width of 1 μm were mimicked by perfectly matched layer (PML) boundary conditions and irradiation of the plane-wave light source and the n and k values of the pollen substrates were obtained using ellipsometric measurements.

Fabrication of Perovskite Solar Cell on Pollen Substrate: The bottom electrode and ETL consisting of 700 nm of zinc oxide/ITO/zinc oxide (ZnO/ITO/ZnO) were deposited on the pollen substrates by DC and RF sputtering. The perovskite layer deposition step involved 1.2 M of a triple cation precursor solution comprising $Cs_{0.05}(MA_{0.17}FA_{0.83})_{0.95}Pb(I_{0.83}Br_{0.17})_3$. A solution was prepared by mixing PbI_2 (1.1×10^{-3} M), FAI (1×10^{-3} M), $PbBr_2$ (0.22×10^{-3} M), and MABr (0.2×10^{-3} M) in 1 mL of a DMF-DMSO (4:1) mixture. Another separate solution of CsI was prepared by mixing 1.5 M CsI in 1 mL of DMSO. Both solutions were heated on a hot plate at 70 °C for a few hours until the solutions were transparent. Next, 42.4 μL of a 1.5×10^{-3} M CsI solution was added to the 1 mL volume of MA-FA (1.2 M) containing the precursor solution. The perovskite solution was spin-coated on the pollen substrate at 3000 rpm for 30 s. A 120 μL volume of chlorobenzene (antisolvent) was dispensed onto the substrate 5 s before the spin cycle stopped. The substrates were then immediately transferred to a hot plate followed by annealing at 100 °C for 30 min. For the hole transfer layer, 50 mg of Spiro-OMeTAD was added in 700 μL of chlorobenzene. 12.4 μL of lithium salt (26 mg lithium bis-(trifluoromethylsulfonyl) imide in 50 μL acetonitrile), 28 μL of cobalt salt (8.5 mg tris (2-(1H-pyrazol-1-yl)-4-tert-butylpyridine)-cobalt(III) tris(bis(trifluoromethylsulfonyl) imide in 28 μL acetonitrile), and 20 μL of 4-tert-Butylpyridine were added to the as-prepared Spiro solution. The solution was heated on a hot plate at 70 °C for 30 min. The Spiro solution was spin-coated onto a perovskite film at 2000 rpm for 30 s. Finally, ≈100 nm of a Ag metal electrode was thermally evaporated on top of the hole transporting material (HTM) layer to complete the device fabrication.

Perovskite Solar Cell Evaluation: The photovoltaic device performance was measured using a Keithley 2401 source meter (Keithley Instruments, Cleveland, OH, USA) with one-sun illumination (XES-40S2 Solar Simulator, San-Ei Electric Co., Ltd., Osaka, Japan).

Supporting Information

Supporting Information is available from the Wiley Online Library or from the author.

Acknowledgements

This research was supported by the MOTIE (Ministry of Trade, Industry, and Energy) in Korea, under the Fostering Global Talents for Innovative Growth Program (P0008746) supervised by the Korea Institute for Advancement of Technology (KIAT). This work was also supported by the SKKU Research Fellowship Program of Sungkyunkwan University and the Ministry of Education, Singapore, under grant AcRF TIER 1-2018-T1-002-115 (RG 173/18). A.S., S.W.L., and L.H.W. acknowledge funding support from the CREATE Programme under the Campus for Research Excellence and Technological Enterprise (CREATE), which was supported by the National Research Foundation, Prime Minister's Office, Singapore.

Conflict of Interest

The authors declare no conflict of interest.

Data Availability Statement

Research data are not shared.

Keywords

biomimetics, energy materials, hierarchical materials, natural materials, optoelectronics

Received: January 21, 2021
Revised: April 6, 2021
Published online:

[1] D. H. Kim, N. Lu, R. Ma, Y. S. Kim, R. H. Kim, S. Wang, J. Wu, S. M. Won, H. Tao, A. Islam, K. J. Yu, T. I. Kim, R. Chowdhury, M. Ying, L. Xu, M. Li, H. J. Chung, H. Keum, M. McCormick, P. Liu, Y. W. Zhang, F. G. Omenetto, Y. Huang, T. Coleman, J. A. Rogers, *Science* **2011**, *333*, 838.
[2] M. S. Lim, M. Nam, S. Choi, Y. Jeon, Y. H. Son, S. M. Lee, K. C. Choi, *Nano Lett.* **2020**, *20*, 1526.
[3] Y. Liu, L. Wang, L. Zhao, K. Yao, Z. Xie, Y. Zi, X. Yu, *Adv. Electron. Mater.* **2019**, *6*, 1901174.
[4] J. J. Norton, D. S. Lee, J. W. Lee, W. Lee, O. Kwon, P. Won, S. Y. Jung, H. Cheng, J. W. Jeong, A. Akce, S. Umunna, I. Na, Y. H. Kwon,

X. Q. Wang, Z. Liu, U. Paik, Y. Huang, T. Bretl, W. H. Yeo, J. A. Rogers, *Proc. Natl. Acad. Sci. USA* **2015**, *112*, 3920.
[5] S. Park, S. W. Heo, W. Lee, D. Inoue, Z. Jiang, K. Yu, H. Jinno, D. Hashizume, M. Sekino, T. Yokota, K. Fukuda, K. Tajima, T. Someya, *Nature* **2018**, *561*, 516.
[6] X. Ren, K. Pei, B. Peng, Z. Zhang, Z. Wang, X. Wang, P. K. Chan, *Adv. Mater.* **2016**, *28*, 4832.
[7] B. Shi, Z. Liu, Q. Zheng, J. Meng, H. Ouyang, Y. Zou, D. Jiang, X. Qu, M. Yu, L. Zhao, Y. Fan, Z. L. Wang, Z. Li, *ACS Nano* **2019**, *13*, 6017.
[8] D. W. Kim, S. Y. Min, Y. Lee, U. Jeong, *ACS Nano* **2020**, *14*, 907.
[9] X. Chen, S. Xu, N. Yao, Y. Shi, *Nano Lett.* **2010**, *10*, 2133.
[10] J. Shen, F. Li, Z. Cao, D. Barat, G. Tu, *ACS Appl. Mater. Interfaces* **2017**, *9*, 14990.
[11] H. Li, W. Wang, Y. Yang, Y. Wang, P. Li, J. Huang, J. Li, Y. Lu, Z. Li, Z. Wang, B. Fan, J. Fang, W. Song, *ACS Nano* **2020**, *14*, 1560.
[12] G. Zhao, Y. Zhang, N. Shi, Z. Liu, X. Zhang, M. Wu, C. Pan, H. Liu, L. Li, Z. L. Wang, *Nano Energy* **2019**, *59*, 302.
[13] Y. Yang, X. Yang, X. Zou, S. Wu, D. Wan, A. Cao, L. Liao, Q. Yuan, X. Duan, *Adv. Funct. Mater.* **2017**, *27*, 1604096.
[14] S. Haghanifar, R. T. Rodriguez De Vecchis, K. J. Kim, J. Wuenschell, S. P. Sharma, P. Lu, P. Ohodnicki, P. W. Leu, *Nanotechnology* **2018**, *29*, 42LT01.
[15] Z. Huang, X. Hu, C. Liu, L. Tan, Y. Chen, *Adv. Funct. Mater.* **2017**, *27*, 1703061.
[16] J. W. Leem, J. S. Yu, *RSC Adv.* **2015**, *5*, 60804.
[17] K. Li, Y. Zhang, H. Zhen, H. Wang, S. Liu, F. Yan, Z. Zheng, *J. Mater. Chem. A* **2017**, *5*, 969.
[18] C. Roldán-Carmona, O. Malinkiewicz, A. Soriano, G. Mínguez Espallargas, A. Garcia, P. Reinecke, T. Kroyer, M. I. Dar, M. K. Nazeeruddin, H. J. Bolink, *Energy Environ. Sci.* **2014**, *7*, 994.
[19] G. Zhao, W. Wang, T. S. Bae, S. G. Lee, C. Mun, S. Lee, H. Yu, G. H. Lee, M. Song, J. Yun, *Nat. Commun.* **2015**, *6*, 8830.
[20] H. Kimura, K. Fukuda, H. Jinno, S. Park, M. Saito, I. Osaka, K. Takimiya, S. Umezu, T. Someya, *Adv. Mater.* **2019**, *31*, 1808033.
[21] M. Ito, Y. Yamashita, Y. Tsuneda, T. Mori, J. Takeya, S. Watanabe, K. Ariga, *ACS Appl. Mater. Interfaces* **2020**, *12*, 56522.
[22] Y. Watanabe, H. Sasabe, J. Kido, *Bull. Chem. Soc. Jpn.* **2019**, *92*, 716.
[23] S. Chen, Y. Song, F. Xu, *ACS Sustainable Chem. Eng.* **2018**, *6*, 5173.
[24] Z. Fang, H. Zhu, Y. Yuan, D. Ha, S. Zhu, C. Preston, Q. Chen, Y. Li, X. Han, S. Lee, G. Chen, T. Li, J. Munday, J. Huang, L. Hu, *Nano Lett.* **2014**, *14*, 765.
[25] Y. Li, M. Cheng, E. Jungstedt, B. Xu, L. Sun, L. Berglund, *ACS Sustainable Chem. Eng.* **2019**, *7*, 6061.
[26] L. Hu, G. Zheng, J. Yao, N. Liu, B. Weil, M. Eskilsson, E. Karabulut, Z. Ruan, S. Fan, J. T. Bloking, M. D. McGehee, L. Wågberg, Y. Cui, *Energy Environ. Sci.* **2013**, *6*, 513.
[27] G. Hou, Y. Liu, D. Zhang, G. Li, H. Xie, Z. Fang, *ACS Appl. Mater. Interfaces* **2020**, *12*, 31998.
[28] C. Jia, C. Chen, Y. Kuang, K. Fu, Y. Wang, Y. Yao, S. Kronthal, E. Hitz, J. Song, F. Xu, B. Liu, L. Hu, *Adv. Mater.* **2018**, *30*, 1801347.
[29] C. Lin, Q. Wang, Q. Deng, H. Huang, F. Huang, L. Huang, Y. Ni, L. Chen, S. Cao, X. Ma, *Cellulose* **2019**, *26*, 4061.
[30] T. F. Fan, S. Park, Q. Shi, X. Zhang, Q. Liu, Y. Song, H. Chin, M. S. B. Ibrahim, N. Mokrzecka, Y. Yang, H. Li, J. Song, S. Suresh, N. J. Cho, *Nat. Commun.* **2020**, *11*, 1449.
[31] F. S. Li, P. Phyo, J. Jacobowitz, M. Hong, J. K. Weng, *Nat. Plants* **2019**, *5*, 41.
[32] V. N. Paunov, G. Mackenzie, S. D. Stoyanov, *J. Mater. Chem.* **2007**, *17*, 609.
[33] J. Seo, L. Wang, W. Ng, N.-J. Cho, *ChemNanoMat* **2016**, *2*, 414.
[34] L. Wang, J. A. Jackman, W. B. Ng, N.-J. Cho, *Adv. Funct. Mater.* **2016**, *26*, 8623.
[35] L. Wang, J. A. Jackman, E.-L. Tan, J. H. Park, M. G. Potroz, E. T. Hwang, N.-J. Cho, *Nano Energy* **2017**, *36*, 38.
[36] L. Wang, W. Ng, J. A. Jackman, N.-J. Cho, *Adv. Funct. Mater.* **2016**, *26*, 2097.
[37] Y. Hwang, M. S. B. Ibrahim, J. Deng, J. A. Jackman, N. J. Cho, *Adv. Funct. Mater.* **2021**, *31*, 2101091.
[38] Z. Zhao, Y. Hwang, Y. Yang, T. Fan, J. Song, S. Suresh, N. J. Cho, *Proc. Natl. Acad. Sci. U. S. A.* **2020**, *117*, 8711.
[39] X. Ma, Q. Deng, L. Wang, X. Zheng, S. Wang, Q. Wang, L. Chen, L. Huang, X. Ouyang, S. Cao, *RSC Adv.* **2019**, *9*, 9348.
[40] C. Gao, S. Yuan, K. Cui, Z. Qiu, S. Ge, B. Cao, J. Yu, *Sol. RRL* **2018**, *2*, 1800175.
[41] S. Castro-Hermosa, J. Dagar, A. Marsella, T. M. Brown, *IEEE Electron Device Lett.* **2017**, *38*, 1278.
[42] M.-H. Jung, N.-M. Park, S.-Y. Lee, *Sol. Energy* **2016**, *139*, 458.
[43] M. Nogi, M. Karakawa, N. Komoda, H. Yagyu, T. T. Nge, *Sci. Rep.* **2015**, *5*, 17254.